

# Functional Geometry of the Permeation Pathway of $\text{Ca}^{2+}$ -activated $\text{Cl}^-$ Channels Inferred from Analysis of Voltage-dependent Block\*

Received for publication, February 8, 2001, and in revised form, February 28, 2001  
Published, JBC Papers in Press, March 9, 2001, DOI 10.1074/jbc.M101264200

Zhiqiang Qu and H. Criss Hartzell‡

From the Department of Cell Biology, Emory University School of Medicine, Atlanta, Georgia 30322-3030

We examined the voltage-dependent block of  $\text{Ca}^{2+}$ -activated  $\text{Cl}^-$  channels by anthracene-9-carboxylic acid (A9C), diphenylamine-2-carboxylic acid (DPC), 4,4'-diisothiocyanostilbene-2,2'-disulfonic acid (DIDS), and niflumic acid (NFA) in excised inside-out and outside-out patches from *Xenopus* oocytes. The fraction of the voltage field ( $\delta$ ) experienced by the blocking drug was determined from the voltage dependence of block. All the drugs blocked by entering the channel from the outside.  $\delta$  was 0.6 for A9C, 0.3 for DPC and DIDS, and  $<0.1$  for NFA. Because the voltage dependence of the drugs differed, the order of potency was also voltage-dependent. At +100 mV the order of potency was  $\text{NFA} > \text{A9C} > \text{DIDS} > \text{DPC}$  ( $K_i$  ( $\mu\text{M}$ ) = 10.1, 18.3, 48, and 111, respectively). Because the drugs are hydrophobic, they can cross the bilayer when applied from the inside and block the channel from the outside. The equilibrium geometries of the blockers were determined by molecular modeling and compared with their blocking positions ( $\delta$ ). This analysis suggests that the channel is an elliptical cone with the largest opening facing the extracellular space. The selectivity filter has an apparent size of  $0.33 \times 0.75$  nm, because  $\text{C}(\text{CN})_3^-$ , which has these dimensions, permeates. The external opening is at least  $0.60 \times 0.94$  nm, because DPC has these dimensions and penetrates the channel  $\sim 30\%$ .

$\text{Ca}^{2+}$ -activated  $\text{Cl}^-$  ( $\text{Cl}(\text{Ca})$ )<sup>1</sup> channels play important roles in physiological processes, including epithelial secretion, repolarization of the cardiac action potential, regulation of vascular tone, olfactory transduction, and neuronal excitability (1–4). *Xenopus* oocytes have long served as a model system for studying  $\text{Cl}(\text{Ca})$  channels because these channels are the predominant channel type natively expressed in this cell and because they are expressed at extremely high levels (0.5 mA/cm<sup>2</sup>) (5). Recently, we have been investigating the mechanisms of anion permeation (6), gating (7), and regulation (8–11) of  $\text{Ca}^{2+}$ -activated  $\text{Cl}^-$  channels in *Xenopus* oocytes, where these channels play a key role in fast block to polyspermy (12). *Xenopus* oocyte  $\text{Cl}(\text{Ca})$  channels have many features in common with  $\text{Cl}(\text{Ca})$  channels in epithelial cells, cardiac myocytes, and vascular smooth muscle cells (see references in Ref. 6), and we think

that elucidating the mechanisms of operation of *Xenopus* oocyte channels will provide important insights into the function of these channels in other tissues.

The roles of  $\text{Cl}(\text{Ca})$  channels in human disease are not yet firmly established. However, there are reasons to think that they may be involved in diseases as diverse as cystic fibrosis and cardiac arrhythmias. For example, there appears to be a reciprocal relationship between the level of expression of CFTR and  $\text{Cl}(\text{Ca})$  channels in airway epithelial cells. Cells from the airway of cystic fibrosis patients can secrete in response to elevations of intracellular  $\text{Ca}^{2+}$  (13, 14), and  $I_{\text{Cl}(\text{Ca})}$  is up-regulated in the airway of CFTR knockout mice (15). The up-regulation of  $I_{\text{Cl}(\text{Ca})}$  in the airway of CFTR knockout mice can apparently compensate for the lack of CFTR and ameliorate the lung pathology in this mouse model (16). Furthermore, overexpression of CFTR in cultured airway epithelial cells from cystic fibrosis patients results in a decrease in  $\text{Cl}(\text{Ca})$  current (17). In the heart, the transient outward current ( $I_{\text{to}}$ ), which plays an important role in repolarization of the cardiac action potential, is composed of several components, one of which ( $I_{\text{to2}}$ ) is mediated by  $\text{Cl}(\text{Ca})$  channels (18–20). Changes in  $I_{\text{to2}}$  can alter cardiac rhythmicity by affecting action potential duration (19, 21). Recently, it has been shown that dogs that are genetically prone to cardiac sudden death have an abnormal  $I_{\text{to}}$  (22), implying that  $\text{Cl}(\text{Ca})$  channels play a role in sudden cardiac death.  $\text{Cl}(\text{Ca})$  channels also contribute to the arrhythmogenic transient inward current ( $I_{\text{ti}}$ ) in some species (22–25). During  $\text{Ca}^{2+}$  overload,  $I_{\text{ti}}$  can trigger oscillatory afterpotentials resulting in serious cardiac arrhythmias (26, 27).  $\text{Cl}^-$  channels clearly can participate in arrhythmogenesis, because anion substitution or pharmacologic  $\text{Cl}^-$  channel blockade protects against reperfusion and ischemia-induced arrhythmias (28–30).

Understanding the nature of the pore of this channel is an important step in elucidating how ions permeate anion-selective channels in general and also in developing reagents that can be used to block or activate these channels. In our previous study (6), we concluded that the pore of the  $\text{Cl}(\text{Ca})$  channel must be at least 0.74 nm in one dimension, because the pseudohalide anion  $\text{C}(\text{CN})_3^-$ , which is  $0.33 \times 0.75$  nm in its smallest cross section, is permeant through the channel. In the present study (6), we have examined the voltage dependence and sidedness of block of several classical  $\text{Cl}^-$  channel blockers and have related these to the molecular size and structure of the blocking molecules. These studies provide insights into the functional geometry of the permeation pathway of this channel.

## EXPERIMENTAL PROCEDURES

**Isolation of *Xenopus* Oocytes**—Stage V–VI oocytes were harvested from adult *Xenopus laevis* females (*Xenopus* I) as described by Dascal (5). *Xenopus* were anesthetized by immersion in tricaine (1.5 g/liter). Ovarian follicles were removed, cut into small pieces, and digested in normal Ringer's solution with no added calcium containing about 2 mg/ml collagenase type IA (Sigma) for 2 h at room temperature. The

\* This work was supported by National Institutes of Health Grant GM 60448. The costs of publication of this article were defrayed in part by the payment of page charges. This article must therefore be hereby marked "advertisement" in accordance with 18 U.S.C. Section 1734 solely to indicate this fact.

‡ To whom correspondence should be addressed. Tel.: 404-727-0444; Fax: 404-727-6256; E-mail: criss@cellbio.emory.edu.

<sup>1</sup> The abbreviations used are:  $\text{Cl}(\text{Ca})$ ,  $\text{Ca}^{2+}$ -activated  $\text{Cl}^-$ ; CFTR, cystic fibrosis transmembrane conductance regulator;  $I$ , current; DIDS, 4,4'-diisothiocyanostilbene-2,2'-disulfonic acid; DPC, diphenylamine-2-carboxylic acid; NFA, niflumic acid; A9C, anthracene-9-carboxylic acid; NMDG, *N*-methyl-D-glucamine.

oocytes were extensively rinsed with normal Ringer's, placed in L-15 medium (Life Technologies, Inc.), and stored at 18 °C. Oocytes were used 1–6 days after isolation. For excised patch experiments, oocytes were placed in a hypertonic solution (200 mM potassium aspartate, 20 mM KCl, 1 mM  $\text{MgCl}_2$ , 10 mM EGTA, 10 mM HEPES, pH 7.2 with KOH) for 1–10 min to facilitate manual removal of the vitelline membrane, and then they were placed in a standard solution (see "Solutions" below) until use.

**Electrophysiological Methods**—Recordings were performed using the inside-out and outside-out excised patch configurations of patch clamp technique. Pipettes were made of borosilicate glass (Sutter Instrument Co.), pulled by a Sutter P-2000 puller, and fire-polished. Patch pipettes had resistances of 6–10 megohms. Unless noted, they were filled with a standard solution (see "Solutions"), which was always the same as the solution in the bath. The bath was grounded via a 3-M KCl-agarose bridge connected to a Ag-AgCl reference electrode. Solution changes were performed by positioning the patch at the end of a battery of sewer pipes having 100- $\mu\text{m}$  internal diameter connected to the gravity feed solution containers. Patches were usually obtained from the animal hemisphere of oocytes, because  $\text{Cl}(\text{Ca})$  channels are concentrated here (9). The patch was typically held at 0 mV, and current was measured in response to a 200-ms voltage ramp from -100 to +100 mV.

Patch clamp data were acquired by an Axopatch 200A amplifier controlled either by Clampex 8.1 via a Digidata 1322A analog-to-digital and digital-to-analog converter (Axon Instruments) or by Curcep 3.0 and a Challenger DB voltage stimulator (W. Goolsby, Emory University).

**Solutions**—Symmetrical solutions containing ~150 mM  $\text{Cl}^-$  were used. In different experiments, the cation was either  $\text{Na}^+$  or NMDG, as indicated in the figure legends.  $\text{Na}^+$  was always used in experiments with 4,4'-diisothiocyanostilbene-2,2'-disulfonic acid (DIDS) because of possible interaction of DIDS and NMDG. The NMDG standard solution contained 150 mM NMDG-Cl, 10 mM NMDG-HEPES, 4 mM  $\text{MgCl}_2$ , pH 7.3. Zero  $\text{Ca}^{2+}$  solution contained 10 mM EGTA. High  $\text{Ca}^{2+}$  solution contained 10 mM EGTA titrated with  $\text{Ca}^{2+}$  to give ~50  $\mu\text{M}$  free  $\text{Ca}^{2+}$ . The standard  $\text{Na}^+$ -containing solution contained 150 mM NaCl, 10 mM HEPES, pH 7.2. Zero  $\text{Ca}^{2+}$  solution contained 10 mM EGTA, and the high  $\text{Ca}^{2+}$  solution contained 0.1 mM  $\text{CaCl}_2$  with no added EGTA. With inside-out patches, to be certain that the currents recorded were  $\text{Ca}^{2+}$ -dependent, we always measured the current in a zero  $\text{Ca}^{2+}$  solution at the start and end of the experiment. If the  $\text{Ca}^{2+}$ -independent current was >5% of the total current in  $\text{Ca}^{2+}$ , the patch was discarded. For outside-out patches, it was not practical to change the  $\text{Ca}^{2+}$  bathing the cytosolic face. Therefore, with outside-out patches, the identity of the current as a  $\text{Cl}^-$  current was verified at the start and end of an experiment by bathing the external face of the patch in solution in which all  $\text{Cl}^-$  was replaced with  $\text{SO}_4^-$ . Patches were not analyzed if the outward current under these conditions was >5% of the current with symmetrical  $\text{Cl}^-$ .

**Anion Channel Blockers**—Diphenylamine-2-carboxylic acid (DPC) and niflumic acid (NFA) were from Sigma; anthracene-9-carboxylic acid (A9C) was from Aldrich; DIDS was from Molecular Probes. DIDS from Sigma and Molecular Probes differed significantly in their color, and some preliminary experiments with Sigma DIDS yielded irreproducible results. DIDS (Molecular Probes) was suspended in water at 0.3 M as a stock before working solutions were made. Other compounds were dissolved in  $\text{Me}_2\text{SO}$  at 0.3 M as stocks to keep the  $[\text{Me}_2\text{SO}]$  in working solutions < 0.1%.

**Display and Analysis of Data**—For the calculations and graphical presentation, we used Origin 6.0 software (Microcal). Curve fitting was performed using the iterative algorithms in Origin. Results are presented as means  $\pm$  S.E., and  $n$  refers to the number of patches in each experiment.

**Molecular Modeling**—The equilibrium geometries of the blockers used were calculated using both MMFF94 molecular mechanics models and Hartree-Fock molecular orbital calculations with the 3-21G\* basis set (31). Calculations were performed using PC Spartan Pro software (Wavefunction, Inc., Irvine, CA) run on an Intel Pentium-III-based PC running Windows 2000. To determine the minimal cross-sectional dimensions of the molecule, the molecule was rotated manually to fit it into the smallest possible rectangle. The center-to-center atomic distances were measured using utilities in PC Spartan Pro; the molecular dimensions were calculated by adding the van der Waals radii of the terminal atoms to the measured center-to-center distances. In the cases of  $\text{C}(\text{CN})_3$  and A9C, the geometries were confirmed by comparison to crystal structure data available in the Cambridge Crystallographic Database.

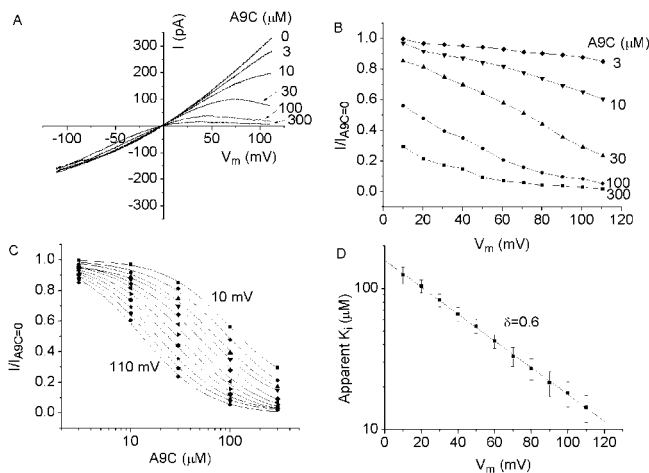


**FIG. 1.  $I_{\text{Cl}(\text{Ca})}$  block by extracellular A9C in an outside-out patch.** *A*,  $I$ - $V$  relationships showing outward  $I_{\text{Cl}(\text{Ca})}$  block by A9C applied to the extracellular side of an outside-out patch. The patch was voltage-clamped from the holding potential of 0 mV with a 250-ms duration voltage ramp from -120 to +120 mV. Both the pipette and the bath contained NMDG standard solution. The extracellular side of the patch was perfused with bath solution containing different concentrations of A9C (0, 3, 10, 30, 100, 300  $\mu\text{M}$ ). *B*, voltage-dependent block of  $I_{\text{Cl}(\text{Ca})}$  by A9C. Each curve from +10 to 110 mV in *A* was divided by the curve obtained in 0  $\mu\text{M}$  A9C. The fractional currents were plotted versus membrane potentials. Note that A9C at every concentration blocks more at the higher voltages. *C*, concentration-dependent block of  $I_{\text{Cl}(\text{Ca})}$ . The fractional currents at various potentials in *B* were replotted as a function of [A9C]. The data were fitted to Equation 1. *D*, apparent  $K_i$  of extracellular A9C as a function of membrane potential. The apparent  $K_i$  at each voltage was determined from the fits in *C* in three separate experiments and averaged. The points were fitted to Equation 2 (the Woodhull equation (32)).

## RESULTS

The goal of these experiments was to characterize the inhibition of  $\text{Ca}^{2+}$ -activated  $\text{Cl}^-$  channels by various  $\text{Cl}^-$  channel blockers. Excised patches in either inside-out or outside-out configurations were pulled from stage VI *Xenopus* oocytes. The solutions on the inside and outside of the patch were always the same, except that 0.1 mM  $\text{CaCl}_2$  was added to the cytosolic face to activate  $\text{Cl}(\text{Ca})$  channels. The effects of the blockers applied to either the cytosolic face of the membrane in inside-out patches or the extracellular face in outside-out patches were then determined.

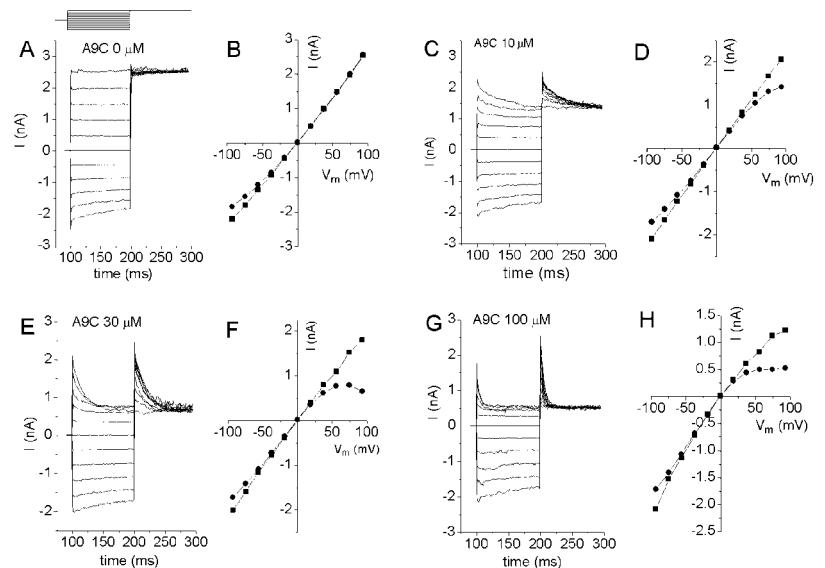
### A9C Blocks from the Outside

**Outside-out Patches**—Fig. 1A shows  $I$ - $V$  curves of  $I_{\text{Cl}(\text{Ca})}$  in an outside-out excised patch from *Xenopus* oocytes recorded with symmetrical 150 mM  $\text{Cl}^-$  solutions. The  $I$ - $V$  curve in the absence of A9C was approximately linear (Fig. 1A). The current was a  $\text{Cl}^-$  current, because the outward current was completely blocked by replacement of extracellular  $\text{Cl}^-$  by impermeant anions such as  $\text{SO}_4^-$ , and replacing  $\text{Na}^+$  with NMDG had little effect on  $E_{\text{rev}}$  (data not shown, but see Ref. 6).

The outward current was blocked in a concentration- and voltage-dependent manner by addition of A9C to the extracellular face of the membrane (Fig. 1A). The inward current was only slightly affected. In Fig. 1B, the currents from Fig. 1A were expressed as a fraction of the current in the absence of A9C ( $I/I_{\text{A9C}=0}$ ) and plotted as a function of voltage. Relative current amplitude decreased with depolarization, confirming that inhibition of  $\text{Cl}^-$  current by A9C was voltage-dependent. The data in Fig. 1B were replotted in Fig. 1C for each voltage as a function of [A9C]. These data were fitted to an equation of the form

$$I/I_{\text{A9C}=0} = I_{\text{min}} + (I_{\text{max}} - I_{\text{min}}) / (1 + ([\text{A9C}]/K_i)^n), \quad (\text{Eq. 1})$$

**FIG. 2. Time dependence of voltage-dependent block by A9C.** The extracellular face of an outside-out patch was exposed to NMDG standard solution (also in pipette) with different [A9C]: 0  $\mu\text{M}$ , *a* and *B*; 10  $\mu\text{M}$ , *c* and *D*; 30  $\mu\text{M}$ , *e* and *F*; 100  $\mu\text{M}$ , *g* and *H*. The patch was voltage-clamped by stepping to various potentials between  $-120$  and  $+120$  mV for 0.1 s with 20-mV increments for each step from the holding potential of 0 mV, followed by a step to  $+120$  mV for 0.1 s (protocol shown above *A*). *A*, *C*, *E*, and *G* show current traces of A9C block. Note that the higher [A9C] made the outward current deactivate faster. *B*, *D*, *F*, and *H* show *I-V* relationships obtained from the corresponding current traces in *A*, *C*, *E*, and *G*, respectively, at 105 ms (closed squares) and 195 ms (closed circles).



where  $I_{\max}$  and  $I_{\min}$  are the maximum and minimum current amplitudes,  $K_i$  is the concentration of A9C required to reduce the current amplitude to  $(I_{\max} + I_{\min})/2$ , and  $n$  is the slope factor.  $K_i$  was determined for each potential and plotted in Fig. 1*D*. The apparent  $K_i$  decreased  $\sim 10$ -fold per 100-mV depolarization. The  $K_i$  at 0 mV was estimated to be 158  $\mu\text{M}$ , and the  $K_i$  at  $+100$  mV was 18.3  $\mu\text{M}$ .

From Fig. 1*D*, one can estimate the fraction of the voltage field experienced by the blocking particle at its blocking site from the equation derived by Woodhull (32, 33),

$$\log K_i(V) = \log K_i(0 \text{ mV}) + (z\delta FV/2.303 RT) \quad (\text{Eq. 2})$$

where  $\log K_i(V)$  is the  $K_i$  at each voltage,  $K_i(0 \text{ mV})$  is the  $K_i$  at 0 mV,  $z$  is the electronic charge of the blocking particle,  $\delta$  is the fraction of the voltage field sensed by the blocker from the outside of the membrane,  $R$ ,  $F$ , and  $T$  have their usual thermodynamic meanings, and  $V$  is voltage. The solid line is the best fit of the antilog of Equation 2 to the data.  $\delta$  was estimated to be  $\sim 0.6$  the distance of the voltage field from the extracellular side.

The inhibition of currents by voltage-dependent blockers is often time-dependent; as membrane potential is changed, the current changes as the blocker accumulates or is removed from the blocking site. Fig. 2 shows  $I_{\text{Cl}(\text{Ca})}$  currents in response to 100-ms duration voltage pulses from a holding potential of 0 mV to voltages between  $+100$  and  $-100$  mV. In the absence of A9C (Fig. 2*A*), outward currents were time-independent. Inward currents at the most negative potentials exhibited a slow decrease in current; currents decreased  $<10\%$  in 100 ms. *I-V* curves were plotted for the current at the beginning (squares) and at the end (circles) of the 100-ms pulses (Fig. 2*B*). Both curves were approximately linear. In the presence of 10  $\mu\text{M}$  A9C (Fig. 2*C*), the outward currents exhibited pronounced time dependence. The currents decayed with time as A9C block developed (Fig. 2*C*), and the *I-V* curves measured at the beginning and end of the voltage pulses diverged at positive potentials. Increasing the [A9C] increased both the rate and the degree of block of the outward current (Fig. 2, *E-H*).

The decay of the current upon stepping from 0 to  $+100$  mV was fitted to a single exponential. The time constants were concentration-dependent;  $\tau = 42.5 \pm 1.2$  ms at 10  $\mu\text{M}$  A9C,  $16.4 \pm 1.1$  ms at 30  $\mu\text{M}$  A9C, and  $11.6 \pm 0.4$  ms at 100  $\mu\text{M}$  A9C ( $n = 3$  for each). These data are consistent with a model in which A9C enters the pore of the channel and blocks it in a voltage-dependent manner.

**Inside-out Patches**—To determine whether A9C also blocked from the inside, we obtained inside-out patches (Fig. 3). Surprisingly, A9C applied from the cytoplasmic side of the patch also blocked outward current (Fig. 3*A*). If A9C had blocked the channel from the inside in a similar manner to block from the outside, we would have expected A9C applied on the cytoplasmic surface to block inward, not outward, current. Woodhull analysis of the voltage-dependent block showed that  $\delta = 0.6$  (Fig. 3*B*). Thus, A9C blocked outward current at the same site in the channel with the same voltage dependence whether it was applied from the inside or outside. The most logical interpretation of these data is that A9C blocks only from the outside but that it crosses the lipid membrane and gains access to the outside when applied from the inside. If this is true, we might expect that the apparent  $K_i$  for block by A9C applied on the inside would be larger than when applied from the outside, because the actual concentration of A9C on the outside when applied from the inside would be lower than expected. In support of this idea, the  $K_i$  for A9C applied to the inside at 0 mV was 945  $\mu\text{M}$  and at  $+100$  mV was 103.7  $\mu\text{M}$ ,  $\sim 5$ – $6$ -fold greater than the  $K_i$  for A9C applied from the outside at the same voltage. In addition, DPC, which has a similar structure to A9C, has been shown to cross lipid membranes readily at neutral pH (see references and “Discussion” in Ref. 34).

#### DPC Blocks from the Outside

A similar analysis was performed for DPC (Fig. 4). In outside-out patches DPC blocked outward current in a dose-dependent manner with an apparent  $K_i$  at 0 mV of 323  $\mu\text{M}$  and at 100 mV of 111  $\mu\text{M}$ . In the experiment illustrated, there was also a small effect on inward current, but it was difficult to determine whether this was a true inhibitory effect or was related to channel rundown, which occurs in some patches.

Woodhull analysis of DPC is presented in Fig. 4, *B-D*. The voltage dependence of the relative current ( $I/I_{\text{DPC} = 0}$ ) in Fig. 4*B* shows that the block by DPC is clearly voltage-dependent. However, the voltage dependence is less than that of A9C (Fig. 1, *C* and *D*).  $\delta$  was estimated to be 0.3. These data show that DPC blocks in a voltage-dependent manner but that the blocking site is not as deep in the pore as the A9C blocking site.

The kinetics of voltage-dependent block by DPC were faster than block by A9C (Fig. 5). Fig. 5, *A* and *B*, shows current traces in response to a series of voltage pulses from 0 mV to voltages between  $-100$  mV and  $+100$  mV for 0 and 300  $\mu\text{M}$  DPC, respectively. Fig. 5*C* shows current traces from the volt-

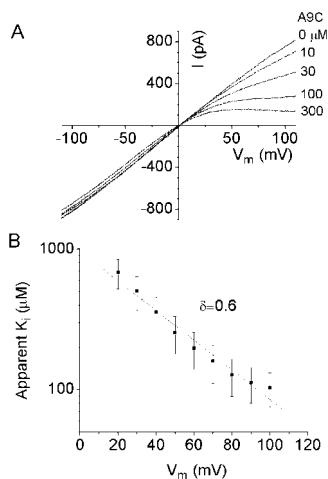


**FIG. 3.  $I_{\text{Cl}(\text{Ca})}$  block by intracellularly applied A9C.** *A*,  $I$ - $V$  relationships showing block of  $I_{\text{Cl}(\text{Ca})}$  by A9C applied to the intracellular side of an inside-out patch. The voltage ramp protocol, solutions, and [A9C] were the same as in Fig. 1. *A*, note that only outward currents were blocked. *B*, apparent  $K_i$  of A9C applied intracellularly versus membrane potentials. Apparent  $K_i$  values were obtained by Woodhull analysis as in the legend to Fig. 1.

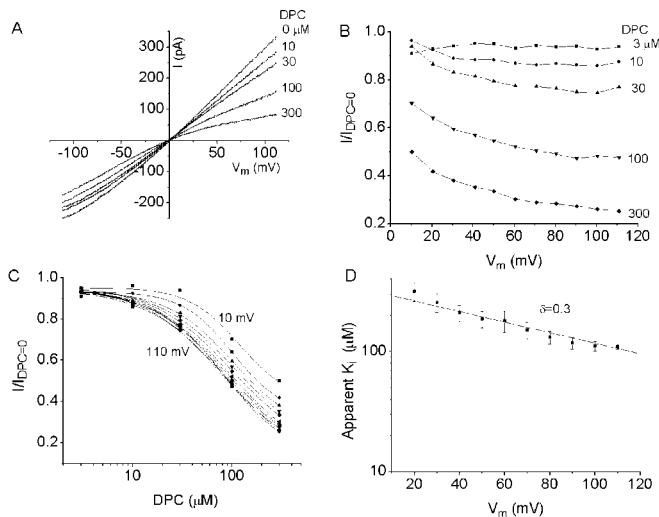


**FIG. 4.  $I_{\text{Cl}(\text{Ca})}$  block by extracellular DPC.** *A*,  $I$ - $V$  relationships showing  $I_{\text{Cl}(\text{Ca})}$  block by DPC in an outside-out patch. *B*, voltage-dependent block of  $I_{\text{Cl}(\text{Ca})}$  by DPC. *C*, concentration-dependent block of  $I_{\text{Cl}(\text{Ca})}$ . *D*, apparent  $K_i$  of extracellular DPC as a function of membrane potential. For details, see the legend to Fig. 1.

age pulses from  $-100$  to  $+100$  mV on a faster time scale for four different DPC concentrations. As [DPC] was increased, a more pronounced time-dependent tail current was observed at the onset of the pulse. The time constant was faster than 1 ms. The  $I$ - $V$  curves showed clearly increasing inward rectification with increasing DPC concentration (Fig. 5*D*).

DPC, like A9C, can cross the membrane when applied from the inside in inside-out patches and block the channel from the outside (Fig. 6). DPC applied from the inside blocked outward current with a  $K_i$  of  $212 \mu\text{M}$  at  $100$  mV, which was about twice the  $K_i$  for inhibition from the outside. The estimated  $\delta$  was 0.2, which was similar to the estimate for DPC applied from the outside. As noted above, DPC has been shown to partition readily into lipid membranes at neutral pH (34).

#### DIDS Blocks from the Outside

*Outside-out*—DIDS applied to the extracellular side decreased outward  $\text{Cl}^-$  current in a dose-dependent manner (Fig. 7*A*). Block was clearly voltage-dependent (Fig. 7*B*). The appar-

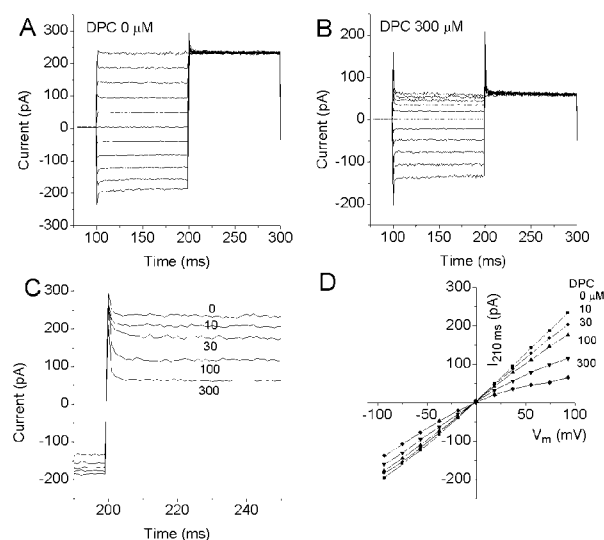


**FIG. 5. Time dependence of  $I_{\text{Cl}(\text{Ca})}$  block by DPC.** An outside-out patch experiment was performed in the same way as in the legend to Fig. 2. The patch was exposed to extracellular DPC at  $0 \mu\text{M}$  DPC (*A*) and  $300 \mu\text{M}$  DPC (*B*). *C*, superimposed current traces elicited by voltage steps from  $-100$  to  $+100$  mV on a faster time scale in different [DPC] as marked. *D*,  $I$ - $V$  relationships for currents measured at 195 ms in *A* and *B*.

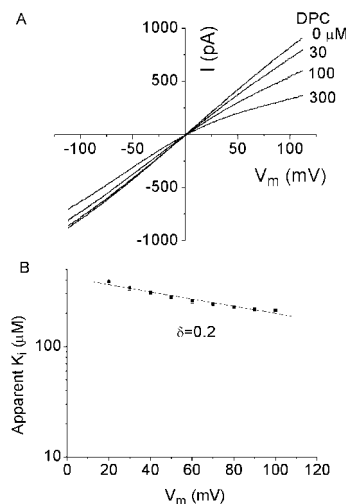


**FIG. 6.  $I_{\text{Cl}(\text{Ca})}$  block by DPC applied intracellularly to inside-out patch.** For experimental conditions refer to the legend to Fig. 3.

ent  $K_i$  at  $0$  mV was  $562 \mu\text{M}$  and at  $+100$  mV was  $48 \mu\text{M}$ .  $\delta$  was estimated to be 0.3 (Fig. 7, *C* and *D*).

*Inside-out*— $100 \mu\text{M}$  DIDS applied to the cytoplasmic side blocked inward current  $>50\%$  and outward current  $\sim 30\%$ , but the block required  $>1$  min to develop (Fig. 8). In contrast, DIDS (and the other blockers used here) applied to outside-out patches produced a steady-state block within several seconds. Because this slowness of block suggested that the mechanisms were significantly different from block from the outside, we did not analyze these results quantitatively.

#### NFA Block Is Not Significantly Voltage-dependent

*Outside-out*—NFA has been widely used to block  $\text{Ca}^{2+}$ -activated  $\text{Cl}^-$  channels in *Xenopus* oocytes (35). In outside-out patches, NFA applied to the extracellular face blocked both inward and outward current (Fig. 9*A*). The apparent  $K_i$  was  $12.9 \mu\text{M}$  at  $0$  mV and  $10.1 \mu\text{M}$  at  $+100$  mV (Fig. 9*D*). Although plots of  $I/I_{\text{NFA}=0}$  versus  $V_m$  (Fig. 9, *B* and *C*) showed some curvature at the highest NFA concentrations, the voltage dependence was rather small. Woodhull analysis (Fig. 9, *C* and *D*)

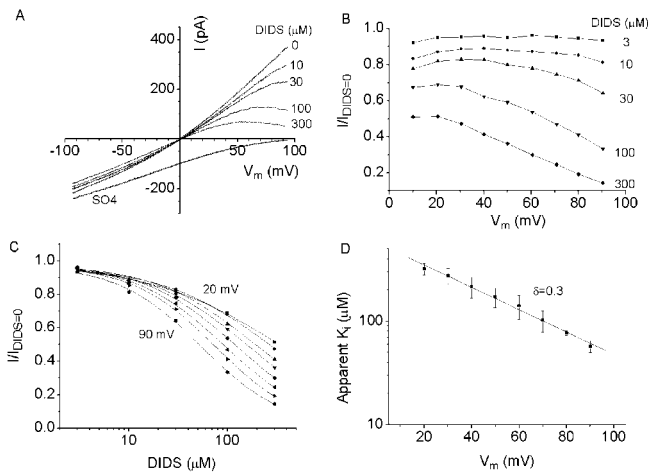


**FIG. 7. Voltage dependence of  $I_{\text{Cl}(\text{Ca})}$  block by external DIDS in outside-out patch.** For all experimental conditions refer to the legend to Fig. 1; however, the cation in these experiments was  $\text{Na}^+$ . *A*,  $I$ - $V$  relationships. *B*, voltage-dependent block by DIDS. *C*, concentration-dependent block by DIDS. *D*, voltage-dependent  $K_i$  of DIDS block.

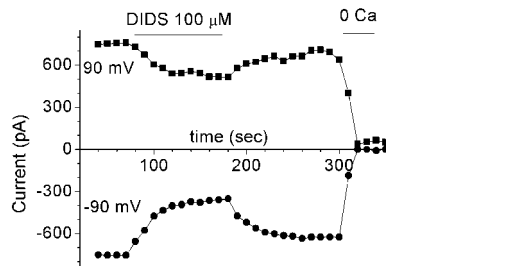


**FIG. 8. Block of current by intracellular DIDS in inside-out patch.** The patch was clamped with a voltage ramp from  $-100$  to  $+100$  mV. The currents at  $-90$  and  $+90$  mV are plotted versus time. The patch was exposed to  $100 \mu\text{M}$  DIDS in  $\text{Na}^+$  standard solution or zero  $\text{Ca}^{2+}$  solution during the periods indicated.

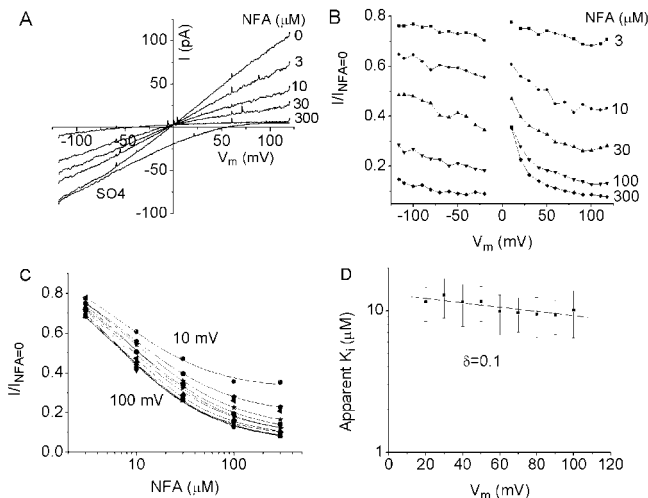


**FIG. 9. Block of  $I_{\text{Cl}(\text{Ca})}$  by external NFA in outside-out patch.** For all experimental conditions refer to the legend to Fig. 1. *A*,  $I$ - $V$  relationships. *B*, voltage-dependent block by NFA. *C*, concentration-dependent block by NFA. *D*, voltage-dependent  $K_i$  of NFA block.

showed that the apparent  $K_i$  did not change significantly between  $20$  mV ( $11.6 \mu\text{M}$ ) and  $100$  mV ( $10.1 \mu\text{M}$ ). The best linear fit to the data in Fig. 9D yielded a small slope that translated into an estimate for  $\delta$  of  $0.1$ .

**Inside-out**—NFA applied to the cytoplasmic face of inside-out patches also blocked both inward and outward current (Fig. 10A) with a  $K_i$  of  $53.7 \mu\text{M}$  at  $+100$  mV (Fig. 10B). This  $K_i$  is

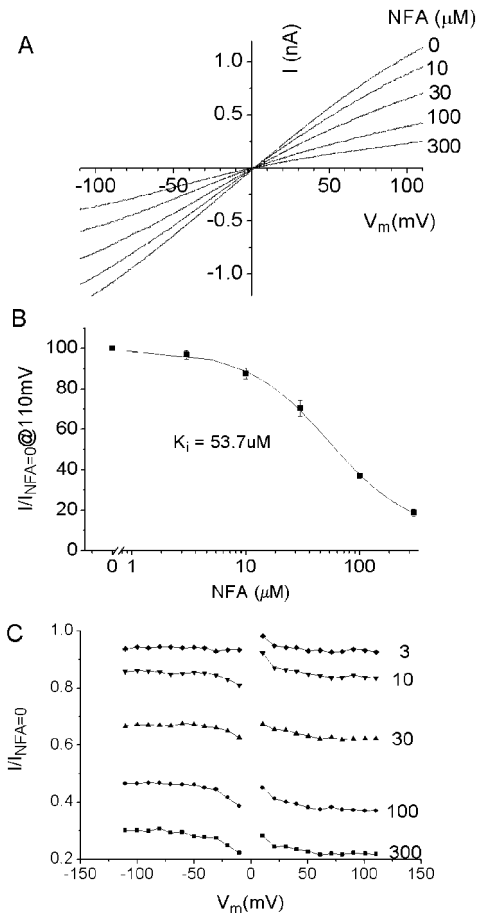


**FIG. 10.  $I_{\text{Cl}(\text{Ca})}$  block by NFA applied intracellularly to inside-out patch.** For experimental conditions refer to the legend to Fig. 3.

about 4 times greater than  $K_i$  for NFA applied from the outside. We do not know whether block of NFA from the inside involves NFA crossing the membrane and blocking from the outside. However, because NFA is very closely related to DPC, we presume that it crosses the membrane readily. There was no voltage dependence to the block (Fig. 10C).

## DISCUSSION

**Summary and Conclusions**—The data on the block of  $\text{Ca}^{2+}$ -activated  $\text{Cl}^-$  channels in *Xenopus* oocytes by various pharmacological agents is summarized in Table I. In outside-out patches, block of  $\text{Cl}^-$  current with externally applied blockers exhibited an order of potency of  $\text{NFA} > \text{A9C} > \text{DIDS} > \text{DPC}$ . Block by NFA was not voltage-dependent, but the blocks by A9C, DIDS, and DPC were voltage-dependent. NFA blocked both inward and outward current, whereas the other blockers blocked only outward current significantly. Block by all four blockers was always reversible under these conditions.

In inside-out patches, block of  $\text{Cl}^-$  currents with blockers applied on the cytosolic side exhibited the order of potency  $\text{NFA} > \text{A9C} > \text{DPC} > \text{DIDS}$ . However, block by A9C and DPC from the inside appeared to be due to the blocker crossing the membrane and blocking from the outside. There are two reasons we conclude that A9C and DPC do not block from the inside. First, these blockers block only outward current, regardless of whether they are applied from the inside or the outside. Second, the  $K_i$  for block from the inside is larger than from the outside. DIDS block from the inside was unusual in that it was very slow. This slow block was not analyzed in detail. Because the block by NFA was only weakly voltage-dependent and because NFA blocked both inward and outward

TABLE I  
 Voltage-dependent block of  $\text{Cl}^-$  currents

The numbers in the parentheses show  $n$  (the number of patches in each experiment);  $K_i$  is in  $\mu\text{M}$ .  $\delta$  is the fraction of the voltage field experienced by the blocker.

	Outside-out			Inside-out		
	$K_i$ (100 mV)	$K_i$ (0 mV)	$\delta$	$K_i$ (100 mV)	$K_i$ (0 mV)	$\delta$
A9C	$18.3 \pm 3.6$ (4)	$158 \pm 17$ (4)	0.6 (3)	$103.7 \pm 28.5$ (3)	$945 \pm 162$ (3)	0.6 (3)
DPC	$111 \pm 9.9$ (3)	$323 \pm 56$ (3)	0.3 (3)	$212.7 \pm 8.2$ (3)	$422 \pm 20$ (3)	0.2 (3)
DIDS	$48 \pm 7.7$ (3)	$562 \pm 39$ (3)	0.3 (3)	N/A <sup>a</sup>	N/A	N/A
NFA	$10.1 \pm 3.7$ (4)	$12.9 \pm 3$ (4)	<0.1 (3)	$53.7 \pm 4.8$ (3)	N/A	N/A

<sup>a</sup> N/A, not applicable.

currents, it was not possible to determine unambiguously the sidedness of NFA block.

These data provide important insights into the functional structure of the pore of the  $\text{Ca}^{2+}$ -activated  $\text{Cl}^-$  channel. Voltage dependence of block is commonly interpreted to reflect binding of the blocker to a site in the anion permeation pathway (33). If this is the case, the calculated fraction of the voltage field ( $\delta$ , from the outside of the channel) experienced by the blocking particle provides an estimate of the position of the blocking site in the channel. We have calculated that  $\delta$  for NFA, DPC, DIDS, and A9C are <0.1, 0.3, 0.3, and 0.6, respectively. This suggests that A9C penetrates further into the pore than DPC and DIDS, which penetrate about the same distance. NFA apparently blocks at a site close to the outside (and possibly the inside) of the channel.

This interpretation depends on the assumption that the drugs block the channel by binding to a site in the permeation pathway. However, because all of the drugs used in this paper are quite hydrophobic, this raises the possibility that these drugs could access a site external to the pore from the lipid phase of the membrane. In the case of A9C and DPC, we think that the data clearly argue against such a mechanism. A9C and DPC block only outward current regardless of whether they are applied to the external or internal side of the membrane. In both cases, the block exhibits the same voltage dependence regardless of the side of the membrane where the drug is applied. These data argue strongly that A9C and DPC must access the channel from the external side and that the block occurs within the permeation pathway. In the case of DIDS and NFA, other interpretations are possible. DIDS block is voltage-dependent, but the sidedness of its effect is ambiguous; although block from the outside is rapid and voltage-dependent, block from the inside is slow and has much weaker voltage dependence. This suggests that DIDS blocks the channel by binding to a site in the permeation pathway when applied from the outside but is capable of blocking the channel by other mechanisms from the inside. Because DIDS is hydrophobic, one might expect that DIDS applied from the outside could reach the “inside” site. However, the access of DIDS to this inside site is quite slow and may not be evident when we rapidly apply DIDS from the outside. NFA blocks current in both directions, and the block is very weakly voltage-dependent, regardless of the side where it is applied. Thus, the possibility exists that NFA blocks the channel in an allosteric manner.

**Functional Model of the  $\text{Ca}^{2+}$ -activated  $\text{Cl}^-$  Channel Pore**—To gain additional insight into the mechanisms of block, we created molecular models of the blocking molecules. The equilibrium geometry of each of the molecules was calculated using molecular orbital calculations (see “Experimental Procedures”). Fig. 11 shows the structures of  $\text{C}(\text{CN})_3$  (the largest anion that we have shown to be permeant through this channel (6)) and the blockers used in this paper. The *left column* of Fig. 11 shows the structures of these molecules viewed from the side. The *right column* of Fig. 11 shows the molecules oriented so that their cross-sectional area is minimized (viewing the

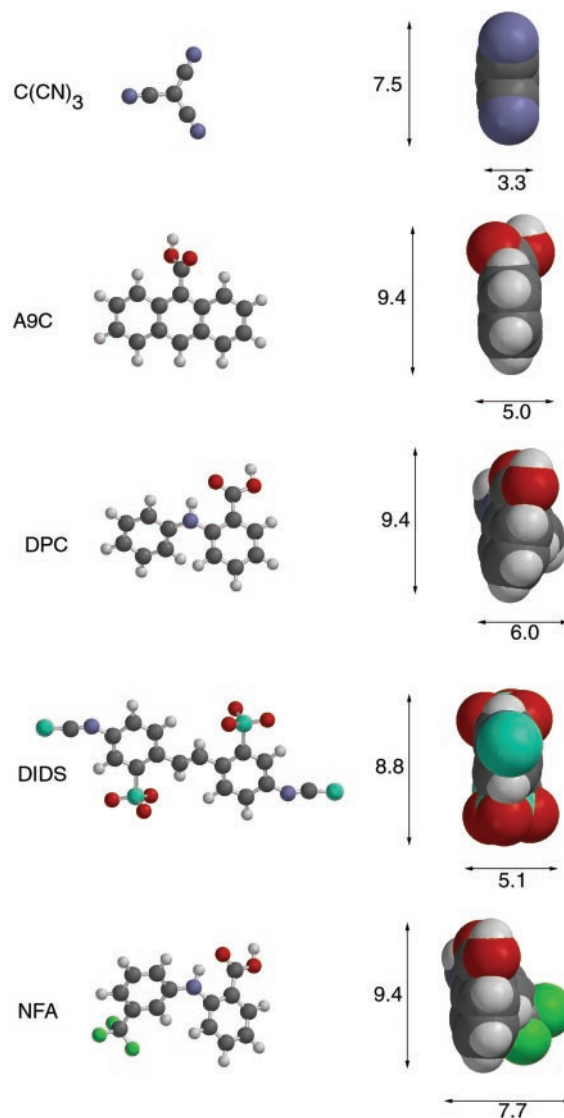


FIG. 11. **Molecular models of  $\text{Cl}^-$  channel blockers and permeant anions.** The equilibrium geometries of the molecules shown were calculated using molecular orbital calculations in PC Spartan Pro. Molecules in the *left column* are shown in ball-and-stick models viewed from the largest cross-sectional area. In the *right column*, the molecules were rotated to show them in their smallest cross-sectional area as space-filling models with the molecular dimensions shown in Å. *Black*, carbon; *white*, hydrogen; *red*, oxygen; *cyan*, sulfur; *green*, fluoride; *blue-gray*, nitrogen.

molecule from the “end”) in a space-filling model with the molecular dimensions shown.

The minimal dimensions of the channel pore can be estimated by comparing the minimal dimensions of the molecules with the estimated distance they penetrate into the channel ( $\delta$ ). We propose that these molecules enter the channel in their

end-on dimension, which is the smallest cross-sectional area. We would argue that if these drugs entered the channel in a different orientation, the pore diameter would be so large that ionic selectivity would be nearly impossible to achieve. In addition, these molecules with rather diverse overall structure exhibit a certain similarity when viewed end-on; their vertical dimensions are rather similar (7.5–9.4 Å). Thus, we propose that in one dimension the channel is at least 7.5 Å for the entire length of the channel. The width of the molecule correlates with  $\delta$ , the depth the blocking molecule penetrates into the channel before it blocks. Because we know that  $\text{C}(\text{CN})_3$  permeates completely through the channel, we conclude that the narrowest part of the pore must be at least as large as  $\text{C}(\text{CN})_3$ , i.e.  $3.3 \times 7.5$  Å. The outer mouth of the channel is at least as large as DPC ( $6.0 \times 9.4$  Å) and may be as large as NFA ( $7.7 \times 9.4$  Å) if NFA blocks within the permeation pathway. However, as noted above, it should be recognized that NFA may not block by entering the permeation pathway but rather allosterically at some other site. A9C enters the channel (voltage field) to a distance about 60% from the outside; so the channel dimensions must be  $\sim 4.6 \times 9.4$  Å at the A9C blocking site. DPC and DIDS only enter about 30% of the way into the channel from the outside; so the dimensions at the DPC and DIDS blocking sites must be  $\sim 6.0 \times 9.4$  Å. The observation that A9C does not block the channel from the inside suggests that the cytosolic opening of the channel is less than  $4.6 \times 9.4$  Å. Thus, the shape of the  $\text{Ca}^{2+}$ -activated  $\text{Cl}^-$  channel permeation pathway approximates an elliptic cone with the largest opening facing the extracellular space. The precision of these estimates is limited by several factors. First, we cannot be certain that the estimate of  $\delta$  is precise, because the width and shape of the voltage field are unknown. Second, the estimates of  $\delta$  probably refer to the fraction of the voltage field experienced by the charge center of the molecule. However, for simplicity we have assumed that this is the same as the geometrical center of the molecule. This assumption seems reasonably well justified because molecular modeling of the charge distribution in these drugs suggests that the charge is either distributed in the molecule or concentrated near the center.

*The Pore of CFTR Is Oriented in the Opposite Polarity to Cl(Ca) Channels*—DPC blocks CFTR from the inside at a site about 60% from the outside surface (36). DIDS does not block from the extracellular side (34) but does block from the intracellular side in a voltage-dependent manner (37). These data suggest that the pore of CFTR is an inverted version of the

Cl(Ca) channel; it appears to have its largest opening on the cytoplasmic side and the smallest opening extracellularly.

*Acknowledgments*—We thank Nael McCarty for helpful discussion and comments and Alyson Ellingson for technical assistance.

## REFERENCES

- Frings, S., Reuter, D., and Kleene, S. J. (1999) *Prog. Neurobiol. (Oxf.)* **60**, 247–289
- Greger, R. (1996) *Pfluegers Arch. Eur. J. Physiol.* **432**, 579–588
- Begenisich, T., and Melvin, J. E. (1998) *J. Membr. Biol.* **163**, 77–85
- Large, W. A., and Wang, Q. (1996) *Am. J. Physiol.* **271**, C435–C454
- Dascal, N. (1987) *CRC Crit. Rev. Biochem.* **22**, 317–387
- Qu, Z., and Hartzell, H. C. (2000) *J. Gen. Physiol.* **116**, 825–844
- Kuruma, A., and Hartzell, H. C. (2000) *J. Gen. Physiol.* **115**, 59–80
- Hartzell, H. C., Machaca, K., and Hirayama, Y. (1996) *Mol. Pharmacol.* **51**, 683–692
- Machaca, K., and Hartzell, H. C. (1998) *Biophys. J.* **74**, 1286–1295
- Machaca, K., and Hartzell, H. C. (1999) *J. Biol. Chem.* **274**, 4824–4831
- Machaca, K., and Hartzell, H. C. (1999) *J. Gen. Physiol.* **113**, 249–266
- Jaffe, L. A., and Cross, N. L. (1986) *Annu. Rev. Physiol.* **48**, 191–200
- Boucher, R. C., Cheng, E. H. C., Paradiso, A. M., Stutts, M. J., Knowles, M. R., and Earp, H. S. (1989) *J. Clin. Invest.* **84**, 1424–1431
- Willumsen, N. J., and Boucher, R. C. (1989) *Am. J. Physiol.* **256**, C226–C233
- Clarke, L. L., Grubb, B. R., Yankaskas, J. R., Cotton, C. U., McKenzie, A., and Boucher, R. C. (1994) *Proc. Natl. Acad. Sci. U. S. A.* **91**, 479–483
- Grubb, B. R., Vick, R. N., and Boucher, R. C. (1994) *Am. J. Physiol.* **266**, C1478–C1483
- Johnson, L. G., Boyles, S. E., Wilson, J., and Boucher, R. C. (1995) *J. Clin. Invest.* **95**, 1377–1382
- Hiraoka, M., and Kawano, S. (1989) *J. Physiol.* **410**, 187–212
- Zygmunt, A. C., Robitelle, D. C., and Eddlestone, G. T. (1997) *Am. J. Physiol.* **273**, H1096–H1106
- Papp, Z., Sipido, K., Callewaert, G., and Carmeliet, E. (1995) *J. Physiol.* **483**, 319–330
- Kawano, S., and Hiraoka, M. (1991) *J. Mol. Cell. Cardiol.* **23**, 681–693
- Freeman, L. C., Pacioretty, L. M., Moise, N. S., Kass, R. S., and Gilmour, R. E., Jr. (1997) *J. Cardiovasc. Electrophysiol.* **8**, 872–883
- Zygmunt, A. C. (1994) *Am. J. Physiol.* **267**, H1984–H1995
- Zygmunt, A. C., Goodrow, R. J., and Weigel, C. M. (1998) *Am. J. Physiol.* **275**, H1979–H1992
- Han, X., and Ferrier, G. R. (1996) *J. Mol. Cell. Cardiol.* **28**, 2069–2084
- Hiraoka, M., Kawano, S., Hirano, Y., and Furukawa, T. (1998) *Cardiovasc. Res.* **40**, 23–33
- January, C. T., and Fozzard, H. A. (1988) *Pharmacol. Rev.* **40**, 219–227
- Curtis, M. J., Garlick, P. B., and Ridley, P. D. (1993) *J. Mol. Cell. Cardiol.* **25**, 417–436
- Ridley, P. D., and Curtis, M. J. (1992) *Circ. Res.* **70**, 617–632
- Tanaka, H., Matsui, S., Kawanishi, T., and Shigenobu, K. (1996) *J. Pharmacol. Exp. Ther.* **278**, 854–861
- Hehre, W. J., Yu, J., Klunzinger, P. E., and Lou, L. (1998) *A Brief Guide to Molecular Mechanics and Quantum Chemical Calculations*, Wavefunction Inc., Irvine, CA
- Woodhull, A. M. (1973) *J. Gen. Physiol.* **61**, 687–708
- Hille, B. (1992) *Ion Channels of Excitable Membranes*, 2nd Ed., Sinauer Associates, Inc., Sunderland, MA
- Schultz, B. D., Singh, A. K., Devor, D. C., and Bridges, R. J. (1999) *Physiol. Rev.* **79**, Suppl. 1, 109–144
- White, M. M., and Aylwin, M. (1990) *Mol. Pharmacol.* **37**, 720–724
- McCarty, N. A., McDonough, S., Cohen, B. N., Riordan, J. R., Davidson, N., and Lester, H. A. (1993) *J. Gen. Physiol.* **102**, 1–23
- Linsdell, P., and Hanrahan, J. W. (1996) *J. Physiol.* **496**, 687–693